ACS APPLIED MATERIALS & INTERFACES

www.acsami.org

Research Article

Integration of the Rhombohedral BiSb(0001) Topological Insulator on a Cubic GaAs(001) Substrate

Dima Sadek, Daya S. Dhungana, Roland Coratger, Corentin Durand, Arnaud Proietti, Quentin Gravelier, Benjamin Reig, Emmanuelle Daran, Pier Francesco Fazzini, Fuccio Cristiano, Alexandre Arnoult, and Sébastien R. Plissard*

Cite This: https://doi.org/10.1021/acsami.1c08477

Read Online

ACCESS | Metrics & More | Article Recommendations | Supporting Information

ABSTRACT: Bismuth−antimony alloy ($Bi_{1-x}Sb_x$) is the first reported 3D topological insulator (TI). Among many TIs reported to date, it remains the most promising for spintronic applications thanks to its large conductivity, its colossal spin Hall angle, and the possibility to build low-current spin-orbit-torque magnetoresistive random access memories. Nevertheless, the 2D integration of TIs on industrial standards is lacking. In this work, we report the integration of high-quality rhombohedral BiSb(0001) topological insulators on a cubic GaAs(001) substrate. We demonstrate a clear epitaxial relationship at the interface, a fully relaxed TI layer, and the growth of a rhombohedral matrix on top of the cubic substrate. The antimony composition of the $Bi_{1-x}Sb_x$ layer is perfectly controlled and covers almost the whole TI window. For optimized growth conditions, the sample generates a semiconductor band structure at room temperature in the bulk and exhibits metallic surface states at 77 K.

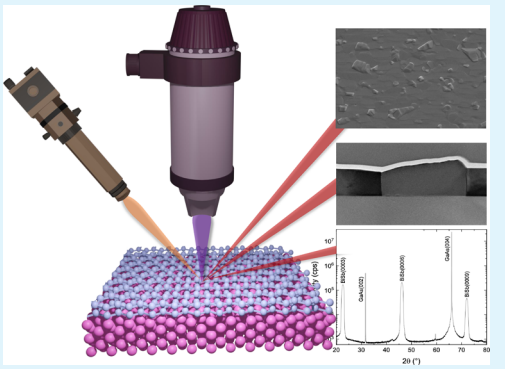

KEYWORDS: *topological insulator, bismuth, antimony, chalcogenide, GaAs*

Topological materials attracted much attention in the last decade due to their unique physical properties. In such condensed matter systems, the electronic surface states are topologically protected from the environment, making them an ideal platform for future quantum devices.[1,2] In their pioneer paper, Kane and Mele predicted the existence of topological insulators (TIs),[3] which are insulators in the bulk and exhibit metallic surface states. These states are topologically protected by time-reversal symmetry and spin−orbit interactions.[4,5] Shortly after this theoretical proposal,[6] TIs were first realized in 2D systems containing HgTe quantum wells[7] and in bismuth−antimony alloys ($Bi_{1-x}Sb_x$) for 3D TIs.[8] Despite numerous TIs being reported thereafter, including most of the chalcogenides,[9−11] $Bi_{1-x}Sb_x$ remains the most promising for spintronic applications thanks to its large conductivity (~10^5 Ω^{-1} m^{-1}),[12,13] its colossal spin Hall angle (~52),[14] and the possibility to build low-current spin-orbit-torque (SOT) magnetoresistive random access memories (MRAM).[15] Moreover, it is possible to control the $Bi_{1-x}Sb_x$ alloy composition and thus to tune precisely its electronic properties. Indeed, $Bi_{1-x}Sb_x$ is predicted to behave as a topological semimetal for $0.04 < x < 0.07$, as a topological insulator[6] for $0.07 < x < 0.22$, or as a Weyl semimetal[16] for $x = 0.5$ or $x = 0.83$. Nevertheless, only a few research groups managed to successfully grow thin epitaxial layers,[17−19] which is a crucial step for industrial integration.

In their recent paper, Yao et al.[18] reported the epitaxial growth of $Bi_{0.73}Sb_{0.27}$ on GaAs(111)A and the texture growth of $Bi_{0.36}Sb_{0.64}$ and $Bi_{0.78}Sb_{0.22}$ on GaAs(001). In this study, the layer growth is strongly affected by surface reconstruction and termination, and the composition barely reaches the TI range. In 2020, two different works presented the growth of BiSb on BaF_2(111) by molecular beam epitaxy (MBE)[17] and on sapphire substrates by a sputtering technique.[19] In the first study, epitaxial BiSb films are obtained by increasing the growth temperature from 150 to 250 °C, which leads to an uncontrolled final Sb composition. In the second one, different grain orientations appear for thicknesses bigger than 50 nm, which affect the layer quality. Finally, a smooth BiSb layer on GaMnAs(001) was grown in 2019 by Khang et al.[20] for lower growth temperature (150 °C), but no claims are reported about wafer-scale homogeneity. Overall, the large lattice mismatches, different crystalline matrices, and difficult surface preparations generate disorders such as strain, cracking, and dislocations. This affects the electronic properties of the

Received: May 10, 2021
Accepted: July 9, 2021

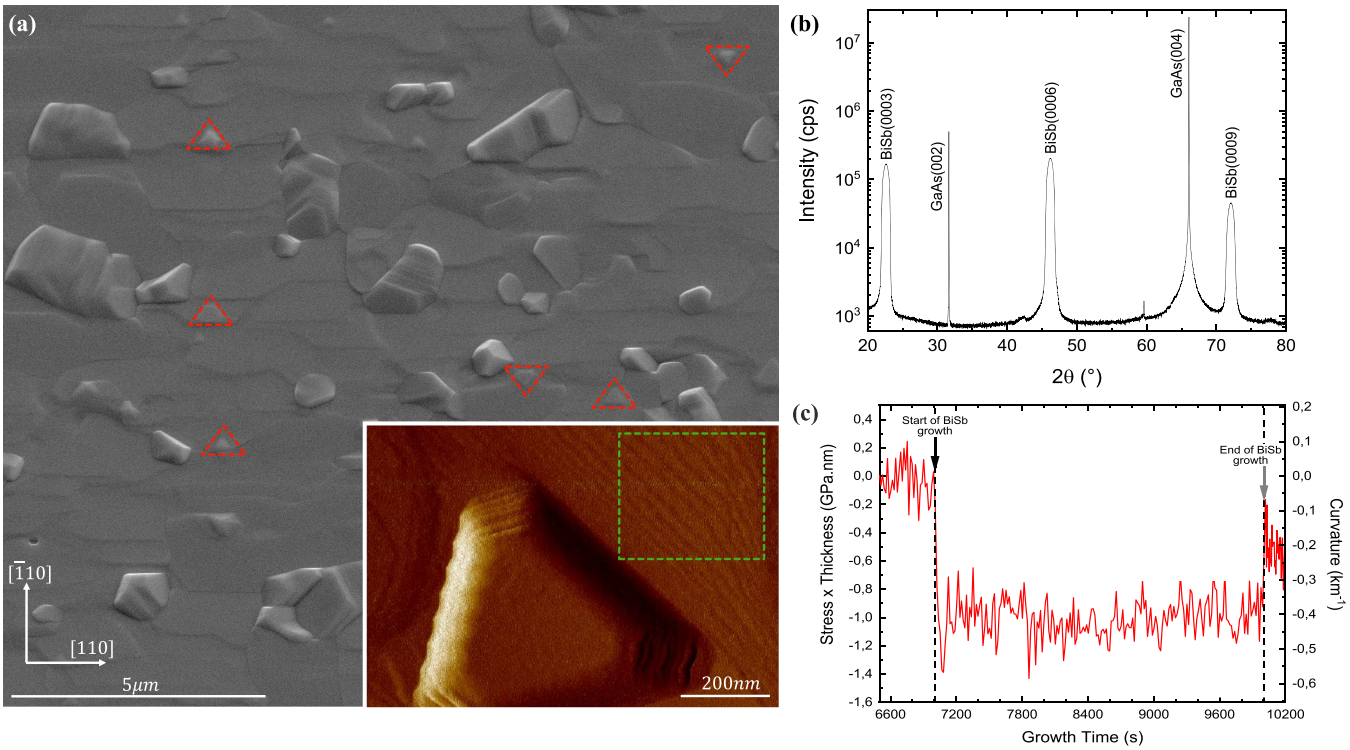

Figure 1. Surface morphology of the as-grown BiSb layer. (a) SEM image and (b) X-ray diffraction of the $Bi_{0.9}Sb_{0.1}$ films deposited on a GaAs(001) substrate. The inset in panel (a) is a high-resolution AFM image of the triangular BiSb grain indicated by the red dashed-triangular shapes. The green dashed-rectangle shows regular layer by layer growth. (c) Stress × thickness and related curvature as a function of growth time. The black and gray arrows indicate the start and end of BiSb growth, respectively. Note that Bi and Sb shutters are opened and closed simultaneously. The stress measurement shows that covalent bonds are formed during the nucleation of BiSb on GaAs: at the start of the BiSb growth, a stress thickness of ∼−1.4 GPa nm appears and relaxes almost immediately (<70 s) during the growth.

$Bi_{1-x}Sb_x$ layer such as the band gap, the mobility, and the effective mass of charge carriers. Such structural defaults can be detrimental for quantum applications since they can destroy the topological protection[21] and even create artifacts such as zero-energy modes in Majorana devices.[22−24]

In this study, we report the epitaxial 2D growth of $Bi_{1-x}Sb_x$ thin films on industrially compatible GaAs substrates by molecular beam epitaxy (MBE). The antimony composition ranges from 5 to 20%, covering almost the whole TI window. Since BiSb has a rhombohedral crystalline structure (R-3m), close to a hexagonal one, a natural substrate could be GaAs(111) as proposed in Yao et al.'s study.[18] Unfortunately, the industrial standards for nanoelectronics and optoelectronics are (001) oriented substrates. Here, we report the growth of this quasi-hexagonal material on a standard GaAs(001) cubic substrate, show a clean epitaxial relationship between GaAs and BiSb, and prove the high quality of the BiSb layer. These hybrid interfaces hold promising properties for MRAM[15] or optical[25] applications.

First, 2 in. undoped GaAs(001) wafers from AXT are loaded in our MBE Riber 412 system and degassed at 300 °C for 1 h. Then, they are deoxidized in a growth chamber at 635 °C under an As flux of 1.2×10^{-5} Torr. A 1 μm-thick GaAs buffer layer is grown with a V/III ratio of 2 at 580 °C. Next, the samples are cooled down to the $Bi_{0.9}Sb_{0.1}$ growth temperature (215 °C), keeping the arsenic flux on for temperatures above 400 °C. During this process, an As-rich GaAs(001) top layer with a c(4 × 4) surface reconstruction[26] is obtained. Finally, Bi and Sb are evaporated simultaneously, and the $Bi_{0.9}Sb_{0.1}$ layer is grown for 50 min, which corresponds to 200 nm. Thanks to an in situ optical monitoring of the wafer curvature,[27] the stress of the system is probed during the growth, as reported in Figure 1c. When Bi and Sb shutters are opened, the stress accumulates for 70 s before reaching a step. Importantly, the presence of stress during nucleation excludes a van der Waals growth process and indicates the creation of covalent bonds between the GaAs(001) substrate and the BiSb(0001) layer.

Figure 1a shows a scanning electron microscopy (SEM) image of an as-grown optimized $Bi_{0.9}Sb_{0.1}$ sample. Different grains can be observed in this figure: the majority has a flat top facet, whereas a few look disoriented. Interestingly, different triangular shapes can be observed (see red dashed lines), always pointing upward or downward (in the [−110] direction), which proves an epitaxial relationship between the GaAs and the BiSb layers. To investigate the crystalline orientation of the grains, X-ray diffraction measurements are performed in a symmetric $2\theta-\omega$ configuration in a Bruker D8 Discover diffractometer. Figure 1b shows the diffraction pattern of the sample presented in Figure 1a. The GaAs(002) and GaAs(004) peaks correspond to the GaAs(001) substrate and the 1 μm-thick buffer layer. The BiSb(0003), BiSb(0006), and BiSb(0009) peaks reveal grains having the same c axis as the GaAs(001) substrate. Importantly, no other grain orientation can be found in this pattern. From Figure 1a,b, it is possible to conclude that most of the $Bi_{0.9}Sb_{0.1}$ grains have a vertical (0001) orientation and thus that the quasi-hexagonal BiSb matrix grows on top of the cubic GaAs one. The inset in Figure 1a shows an amplitude error AFM image of a triangular grain obtained by stacking several triangular layers (see the Supporting Information,

https://doi.org/10.1021/acsami.1c08477
ACS Appl. Mater. Interfaces XXXX, XXX, XXX−XXX

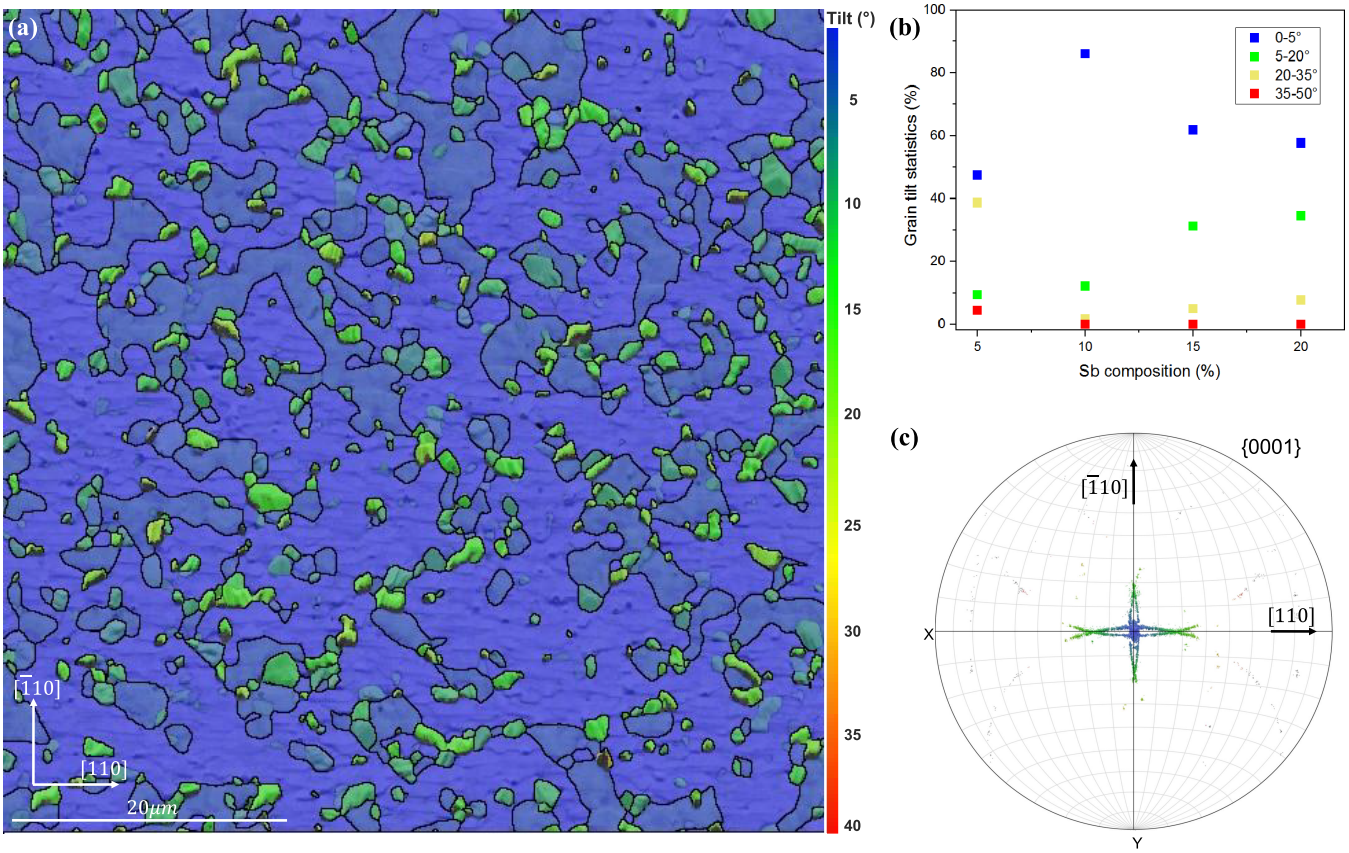

Figure 2. Determination of the grain orientation. (a) EBSD map showing the angular deviation between the (0001) $Bi_{0.9}Sb_{0.1}$ grains and the GaAs(001) substrate. The color scale corresponds to the tilt ranging from 0 to 40° with respect to the substrate direction. (b) Grain tilt statistics as a function of Sb composition (5, 10, 15, and 20%). (c) Corresponding pole figure displaying the (0001) grain orientation and showing distribution with respect to the [110] and [$\bar{1}$10] GaAs directions.

Figure SI-2 for the corresponding 3D height sensor image). This extremely sensitive AFM mode corresponds to the difference between the oscillation amplitude of the tip and the preset amplitude value. It allows determining precisely the shape of the topographical surface features. Here, the top facet of the terrace is flat without any step, and no screw dislocation can be observed. A regular array of steps can be observed in the green area of the inset of Figure 1a, starting from the side of the triangular grain and covering the substrate.

In order to investigate the crystalline orientation and the size distribution of the $Bi_{0.9}Sb_{0.1}$ grains, an electron backscattering diffraction (EBSD) measurement was performed in a FEG-SEM JEOL JSM 7100F equipped with a Nordlys Nano EBSD camera (Oxford Instruments). Figure 2a shows the EBSD map and the tilt of $Bi_{0.9}Sb_{0.1}$ (0001) grains with respect to the GaAs substrate [001] direction. The color scale on the right of Figure 2a corresponds to tilts ranging from 0 to 40°. The surface fraction indexed region (colored surface in Figure 2a) represents 97.8% of the EBSD map; thus, most of the grain orientations are determined. Unindexed regions are localized mainly at grain boundaries. In order to study this orientation as a function of the antimonide composition, three other samples are grown with x compositions of 5, 15, and 20%, keeping all other parameters constant. Statistics about the grain orientation for the different compositions are reported in Figure 2b. Four grain families are defined as follows: in blue, grains having a tilt between 0 and 5°; in green, a tilt between 5 and 20°; in yellow, a tilt between 20 and 35°; and finally in red, a tilt between 35 and 50°. First, it can be noticed that the growth conditions are clearly optimized for the $Bi_{0.9}Sb_{0.1}$ sample (Figures 1 and 2a) since 84.2% of the grains are (0001) oriented and have less than 5° of tilt. About 12% have a tilt between 5 and 20°, and less than 4% of the total substrate surface has other grain orientations. Furthermore, it can be observed that the grain size is directly dependent on its orientation: when the tilt is below 5°, the mean grain size is 3.93μm^2, whereas it is 0.88μm^2 for larger tilts. On the other hand, the surface morphology for the other compositions (see the Supporting Information, Figure SI-3) is rougher and less organized and presents more holes. If low tilt grains (in blue) represent the majority of the surface for all compositions, other grain orientations are favored when changing x: more bismuth favors grains having a tilt around 25° (in yellow), whereas more antimonide favors 10° tilt grains (in green). Finally, an EBSB pole figure of the $Bi_{0.9}Sb_{0.1}$ sample is presented in Figure 2c. The x axis corresponds to the [110] direction of the GaAs substrate, whereas the y axis corresponds to the [−110] one. It can be noticed that the tilt distribution is not random: a cross is formed in the center of the pole figure, which reveals two preferential tilting directions: either the [110] or the [−110] direction. It is unlikely for a grain to tilt along any other directions, which indicates a clear epitaxial relationship and covalent bonds between the BiSb layer and the GaAs substrate. This is further confirmed by the XRD pole figure reported in Figure SI-4 and performed on the same sample.

https://doi.org/10.1021/acsami.1c08477
ACS Appl. Mater. Interfaces XXXX, XXX, XXX−XXX

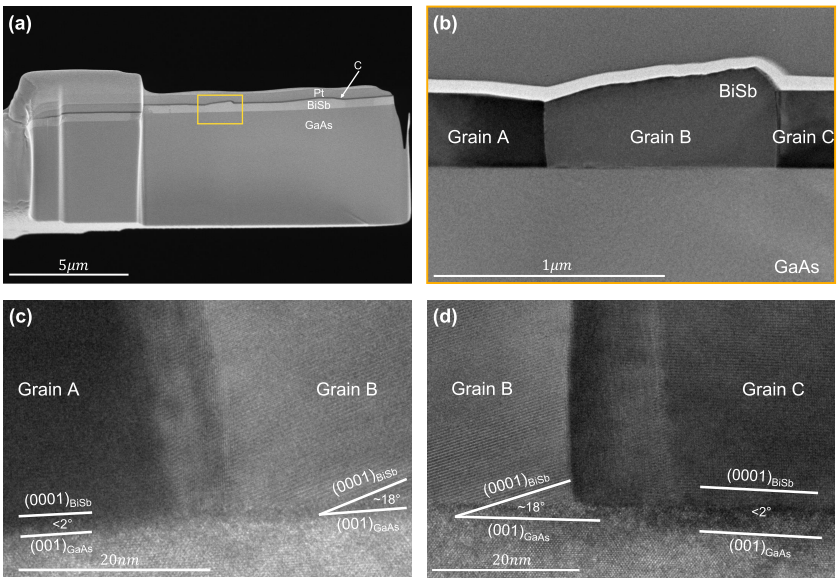

Figure 3. Cross-sectional measurement of the sample. (a) SEM image of the FIB cut once carbon and platinum have been deposited. (b) Zoomed TEM images of the BiSb/GaAs interface indicated by a yellow square in panel (a) and showing the existence of different grains (A, B, and C). (c) Boundary between grains A and B. (d) Boundary between grains B and C.

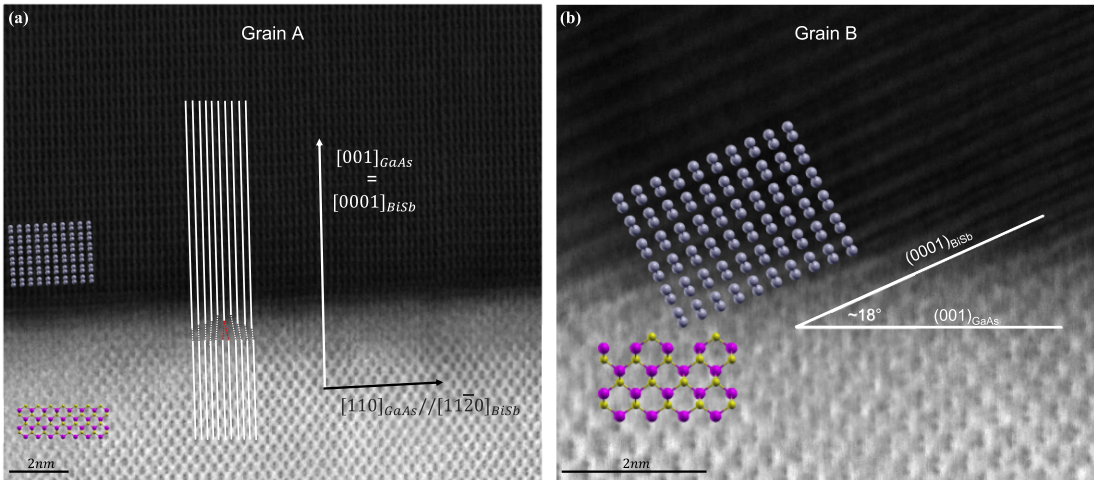

Figure 4. Interface between the BiSb layer and the GaAs substrate. The HR-TEM images are taken in the [1$\bar{1}$0] zone axis of the GaAs and show the interface between GaAs and grain A in panel (a) and grain B in panel (b). The grain growth direction is [0001] with a tilt less than 2° for grain A and of 18° for grain B. 90° dislocations are detected at the grain A/GaAs interface indicated by red dashed lines in panel (a). The inset images in panels (a) and (b) show the side views of the crystal structures of grain A, grain B, and GaAs(001). Bi, As, and Ga atoms are represented by gray, yellow, and pink atoms, respectively.

In order to probe the BiSb/GaAs interface and to assess the crystalline quality of the optimized $Bi_{0.9}Sb_{0.1}$ layer (see Figure 2), a thin lamella of the sample, obtained by focused ion beam (FIB), was examined by transmission electron microscopy (TEM) (Figure 3). In order to protect the sample, a layer of carbon and another of platinum are deposited on top of the BiSb layer prior to the FIB cut, as illustrated in the SEM image of the lamella reported in Figure 3a. To further study the BiSb/GaAs interface, a zoomed TEM image is shown in Figure 3b, where three grains A, B, and C can be observed. In addition, high-resolution images of the interface between the three grains and the GaAs substrate are reported in Figure 3c,d. Noticeably, grains A and C have a rather flat surface (cf. Figure 3a), while their (001) plane rows are almost parallel to the GaAs ones (<2° in Figure 3c,d). On the contrary, the B grain surface is rough, and its (001) planes are inclined with respect to the GaAs ones (~18° in Figure 3c,d). Moreover, the grain boundaries are mostly vertical as shown in Figure 3c,d, and a low strain can be observed at their junction. No further structural defects can be observed in any of the grains, proving their high structural quality.

In order to gain knowledge about their crystalline structure and the BiSb/GaAs interface, high-resolution transmission electron microscopy (HR-TEM) measurements were performed on grain A (Figure 4a) and grain B (Figure 4b). In the case of grain A, the [0001] growth direction is confirmed by Figure 4a. A low tilt can be observed (<2°) between the GaAs substrate and the BiSb layer, which corresponds to the blue family in Figure 2b. The [110] direction of the GaAs corresponds to the [11−20] of the BiSb, and the *c* axis is identical for both crystals. 90° dislocations are present at the interface (see the red dashed line), and the BiSb grain is fully

https://doi.org/10.1021/acsami.1c08477
ACS Appl. Mater. Interfaces XXXX, XXX, XXX−XXX

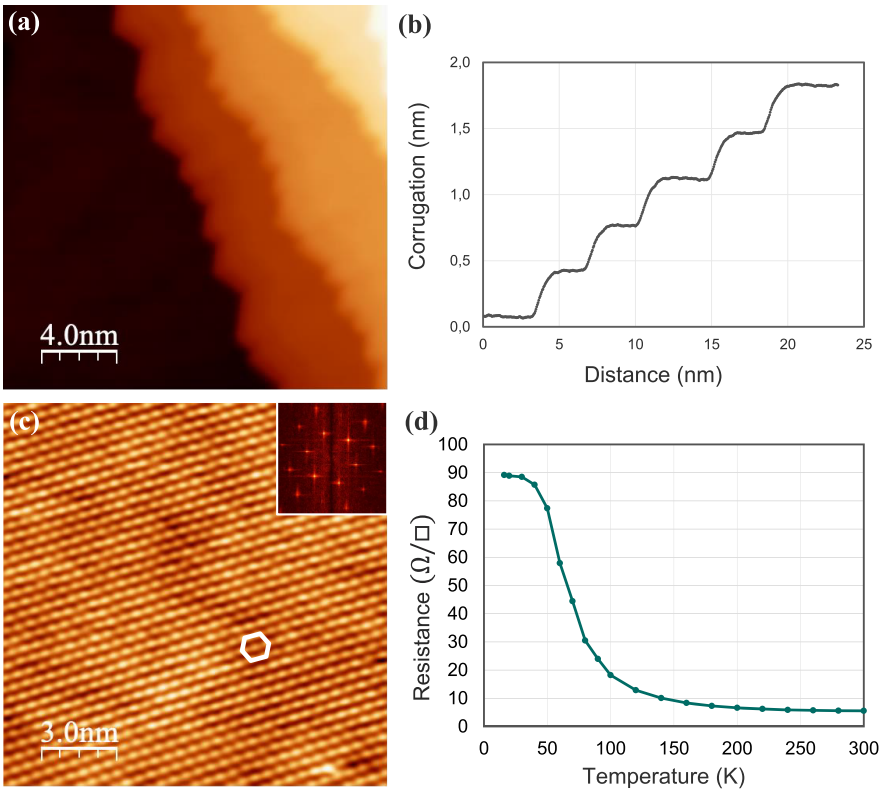

Figure 5. STM measurements of the surface. (a) Large-scale STM topography (20 × 20 nm^2) of the BiSb surface (V = 1 V, I = 10 pA, and T = 77 K). The steps on the right are monoatomic and present characteristic kinks. (b) Typical cross section performed across monoatomic steps separating small terraces. (c) Atomic resolution on a BiSb terrace (15 × 15 nm2) showing the hexagonal network (V = 1 V, I = 10 pA, and T = 77 K). In the inset: a characteristic FFT pattern of a large-scale STM image (20 × 20 nm^2) with atomic resolution conducted on the BiSb surface. From the central hexagonal pattern, a lattice parameter of 4.4 ± 0.4 Å can be obtained. (d) Sheet resistance of the 450 nm-thick $Bi_{0.9}Sb_{0.1}$ sample as a function of temperature.

relaxed. On the contrary, for grain B, an 18° tilt can be observed between the GaAs [001] and the BiSb [0001] directions (Figure 4b). These measurements are in good agreement with both the XRD measurements in Figure 1b and the EBSD one in Figure 2a,b. The BiSb layer is fully relaxed, covalent bonds are formed during BiSb nucleation, and each grain has a high structural quality.

Finally, in order to investigate the $Bi_{0.9}Sb_{0.1}$ surface topography, scanning tunneling microscopy (STM) experiments were performed at liquid nitrogen temperature (T = 77.8 K) on a commercial STM (LT Omicron), working with a base pressure of 3 × 10^{-11} mbar. Further details about the measurement are given in the Supporting Information (Text SI-6). Figure 5a shows a 20 × 20 nm^2 STM image of a BiSb terrace (on the left) and a stepped area (on the right). The step edges present a characteristic kink that demonstrates the perfect film crystallinity. The larger terraces observed can be several thousand of nanometers large on top of the crystallites. These large domains are surrounded by stepped areas as presented in Figure 5a, corresponding to the sides of these crystallites. The corrugated areas can be used to measure the monoatomic step height. A profile across a step band is presented in Figure 5b. The cross section performed on another large-scale image shows the presence of small terraces about 2 nm wide separated by monoatomic steps, whose average height is 3.56 ± 0.4 Å, which corresponds to one-third of the c $Bi_{0.9}Sb_{0.1}$ lattice parameter at 77 K (1/3 of 11.76 Å at 77 K).[28,29] The surface of a terrace with atomic resolution is presented in Figure 5c. The used bias voltage is 600 mV, and the tunneling current is 5 pA. As expected, the Bravais lattice is hexagonal (see the white hexagon superimposed on the atomic network in Figure 5c). The lattice parameters can be measured from this kind of image or from fast Fourier transform (FFT) performed on larger scale topographies with atomic resolution. A typical example is presented in the inset of Figure 5c and shows the characteristic diffraction pattern. From these measurements, a lattice parameter of 4.4 ± 0.4 Å is obtained, close to the theoretical 4.51 Å for a fully relaxed $Bi_{0.9}Sb_{0.1}$ layer at 77 K.[29] Another point concerns the bias voltage that can be used in the STM experiments. During the STM investigations, it appears that very reproducible surface topographies can be obtained for bias voltages as low as 40 mV (for tunneling currents in the picoampere range). This suggests a large conductivity of the $Bi_{0.9}Sb_{0.1}$ layer at liquid nitrogen temperature, which is consistent with a metallic surface.

In addition, resistivity measurements have been performed on a 450 nm-thick $Bi_{0.9}Sb_{0.1}$ sample by the four-terminal method with a van der Pauw configuration. As shown in Figure 5d, the sheet resistance increases while decreasing the temperature from 300 to 16 K, characteristic of a semiconducting bulk, and tends to reach a plateau below 30 K. From Hall measurements, we observed an n-type semiconductor behavior of the bulk with a carrier density of 5 × 10^{19}cm^{-3} (9 × 10^{18}cm^{-3}) and an electron mobility of 520 cm^2/V · s (1200 cm^2/V · s) at 300 K (at 100 K). Both measurements prove the good electrical properties of the BiSb layer and the semiconductor behavior of the bulk, whereas STM measurements indicate metallic surface states. Overall,

https://doi.org/10.1021/acsami.1c08477
ACS Appl. Mater. Interfaces XXXX, XXX, XXX−XXX

our electrical measurements are compatible with the behavior of a topological insulator.[30]

In conclusion, we achieved the growth of high-quality BiSb thin films on GaAs(001) despite large mismatches and different crystalline matrices. We found that optimized growth conditions yield more than 80% of the grains having a negligible tilt with the substrate. A clear epitaxial relationship is found between the GaAs and the BiSb. The surface roughness and disorder are reduced, and the BiSb thin film is fully relaxed. These results are confirmed by SEM, AFM, EBSD, HR-TEM, and STM characterizations. Finally, electrical measurements prove the high quality of the BiSb layer, a semiconductor behavior at room temperature in the bulk, and metallic surface states at 77 K.

■ ASSOCIATED CONTENT

Supporting Information

The Supporting Information is available free of charge at https://pubs.acs.org/doi/10.1021/acsami.1c08477.

SEM and AFM images of a thin BiSb layer grown on a GaAs(001) substrate. XRD pole figure of the BiSb layer on the GaAs(001) substrate. FIB preparation of the TEM lamella and cross-sectional SEM images. Description of the STM and of the Hall effect measurements (PDF)

■ AUTHOR INFORMATION

Corresponding Author

Sébastien R. Plissard − *LAAS-CNRS, Université de Toulouse, Toulouse F-31400, France*; orcid.org/0000-0002-0769-5429; Email: sebastien.plissard@laas.fr

Authors

Dima Sadek − *LAAS-CNRS, Université de Toulouse, Toulouse F-31400, France*

Daya S. Dhungana − *LAAS-CNRS, Université de Toulouse, Toulouse F-31400, France*

Roland Coratger − *SINANO Group, CEMES-CNRS and Université Paul Sabatier, Toulouse 31055, France*

Corentin Durand − *LAAS-CNRS, Université de Toulouse, Toulouse F-31400, France; SINANO Group, CEMES-CNRS and Université Paul Sabatier, Toulouse 31055, France*

Arnaud Proietti − *Centre De Microcaractérisation Raimond Castaing, Toulouse F-31400, France*

Quentin Gravelier − *LAAS-CNRS, Université de Toulouse, Toulouse F-31400, France*

Benjamin Reig − *LAAS-CNRS, Université de Toulouse, Toulouse F-31400, France*

Emmanuelle Daran − *LAAS-CNRS, Université de Toulouse, Toulouse F-31400, France*

Pier Francesco Fazzini − *Laboratoire de Physique et Chimie des Nano-objets, Institut National des Sciences Appliquées, Toulouse F-31077, France*

Fuccio Cristiano − *LAAS-CNRS, Université de Toulouse, Toulouse F-31400, France*

Alexandre Arnoult − *LAAS-CNRS, Université de Toulouse, Toulouse F-31400, France*

Complete contact information is available at: https://pubs.acs.org/10.1021/acsami.1c08477

Author Contributions

D.S. and S.R.P. conceived the project and experiments. D.S, D.S.D., A.A., and S.R.P. grew the samples. D.S. and E.D. performed the AFM measurements. A.P. performed the EBSD one, and B.R. performed the FIB preparation. R.C. and C.D. measured the samples in the STM, P.F.F. and F.C. measured the samples in the TEM. Q.G. performed Hall measurements. D.S., R.C., C.D., A.A., and S.R.P. analyzed the measurements and wrote the manuscript with input from all the authors.

Funding

This work is funded by the Agence National de la Recherche (ANR) under grant number ANR-17-PIRE-0001 (HYBRID project).

Notes

The authors declare no competing financial interest.

■ ACKNOWLEDGMENTS

This study benefited from the support of the LAAS-CNRS micro and nanotechnologies platform, which is a member of the French RENATECH network.

■ REFERENCES

(1) Moore, J. E. The Birth of Topological Insulators. *Nature* **2010**, *464*, 194−198.

(2) Tang, S.; Dresselhaus, M. S. Electronic Properties of Nano-Structured Bismuth-Antimony Materials. *J. Mater. Chem. C* **2014**, *2*, 4710−4726.

(3) Kane, C. L.; Mele, E. J. Z_2 Topological Order and the Quantum Spin Hall Effect. *Phys. Rev. Lett.* **2005**, *95*, 146802.

(4) Young, S. M.; Chowdhury, S.; Walter, E. J.; Mele, E. J.; Kane, C. L.; Rappe, A. M. Theoretical Investigation of the Evolution of the Topological Phase of Bi_2 Se_3 under Mechanical Strain. *Phys. Rev. B* **2011**, *84*, No. 085106.

(5) Hasan, M. Z.; Kane, C. L. Colloquium: Topological Insulators. *Rev. Mod. Phys.* **2010**, *82*, 3045−3067.

(6) Fu, L.; Kane, C. L. Topological Insulators with Inversion Symmetry. *Phys. Rev. B* **2007**, *76*, No. 045302.

(7) Bernevig, B. A.; Hughes, T. L.; Zhang, S.-C. Quantum Spin Hall Effect and Topological Phase Transition in HgTe Quantum Wells. *Science* **2006**, *314*, 1757.

(8) Hsieh, D.; Qian, D.; Wray, L.; Xia, Y.; Hor, Y. S.; Cava, R. J.; Hasan, M. Z. A Topological Dirac Insulator in a Quantum Spin Hall Phase. *Nature* **2008**, *452*, 970−974.

(9) Kuroda, K.; Ye, M.; Kimura, A.; Eremeev, S. V.; Krasovskii, E. E.; Chulkov, E. V.; Ueda, Y.; Miyamoto, K.; Okuda, T.; Shimada, K.; Namatame, H.; Taniguchi, M. Experimental Realization of a Three-Dimensional Topological Insulator Phase in Ternary Chalcogenide $TlBiSe_2$. *Phys. Rev. Lett.* **2010**, *105*, 146801.

(10) Jin, H.; Song, J.-H.; Freeman, A. J.; Kanatzidis, M. G. Candidates for Topological Insulators: Pb-Based Chalcogenide Series. *Phys. Rev. B* **2011**, *83*, No. 041202.

(11) Fornari, C. I.; Rappl, P. H. O.; Morelhão, S. L.; Abramof, E. Structural Properties of Bi2Te3 Topological Insulator Thin Films Grown by Molecular Beam Epitaxy on (111) BaF2 Substrates. *J. Appl. Phys.* **2016**, *119*, 165303.

(12) Kozhemyakin, G. N.; Zayakin, S. A. Magnetoresistance in Doped $Bi_{0.85}Sb_{0.15}$ Single Crystals. *J. Appl. Phys.* **2017**, *122*, 205102.

(13) Qu, D.-X.; Roberts, S. K.; Chapline, G. F. Observation of Huge Surface Hole Mobility in the Topological Insulator $Bi_{0.91}$ $Sb_{0.09}$ (111). *Phys. Rev. Lett.* **2013**, *111*, 176801.

(14) Khang, N. H. D.; Ueda, Y.; Hai, P. N. A Conductive Topological Insulator with Large Spin Hall Effect for Ultralow Power Spin−Orbit Torque Switching. *Nat. Mater.* **2018**, *17*, 808−813.

(15) Khang, N. H. D.; Nakano, S.; Shirokura, T.; Miyamoto, Y.; Hai, P. N. Ultralow Power Spin−Orbit Torque Magnetization Switching

Induced by a Non-Epitaxial Topological Insulator on Si Substrates. *Sci. Rep.* **2020**, *10*, 12185.
(16) Su, Y.-H.; Shi, W.; Felser, C.; Sun, Y. Topological Weyl Semimetals in $Bi_{1-x}Sb_x$ Alloys. *Phys. Rev. B* **2018**, *97*, 155431.
(17) Ueda, K.; Hadate, Y.; Suzuki, K.; Asano, H. Fabrication of High-Quality Epitaxial Bi1-XSbx Films by Two-Step Growth Using Molecular Beam Epitaxy. *Thin Solid Films* **2020**, *713*, 138361.
(18) Yao, K.; Khang, N. H. D.; Hai, P. N. Influence of Crystal Orientation and Surface Termination on the Growth of BiSb Thin Films on GaAs Substrates. *J. Cryst. Growth* **2019**, *511*, 99−105.
(19) Fan, T.; Tobah, M.; Shirokura, T.; Huynh Duy Khang, N.; Nam Hai, P. Crystal Growth and Characterization of Topological Insulator BiSb Thin Films by Sputtering Deposition on Sapphire Substrates. *Jpn. J. Appl. Phys.* **2020**, *59*, No. 063001.
(20) Duy Khang, N. H.; Hai, P. N. Giant Unidirectional Spin Hall Magnetore-sistance in Topological Insulator - Ferromagnetic Semiconductor Hetero-structures. *J. Appl. Phys.* **2019**, *126*, 233903.
(21) Fadaly, E. M. T.; Zhang, H.; Conesa-Boj, S.; Car, D.; Gül, Ü.; Plissard, S. R.; Op het Veld, R. L. M.; Kölling, S.; Kouwenhoven, L. P.; Bakkers, E. P. A. M. Observation of Conductance Quantization in InSb Nanowire Networks. *Nano Lett.* **2017**, *17*, 6511−6515.
(22) Chen, J.; Woods, B. D.; Yu, P.; Hocevar, M.; Car, D.; Plissard, S. R.; Bakkers, E. P. A. M.; Stanescu, T. D.; Frolov, S. M. Ubiquitous Non-Majorana Zero-Bias Conductance Peaks in Nanowire Devices. *Phys. Rev. Lett.* **2019**, *123*, 107703.
(23) Su, Z.; Zarassi, A.; Hsu, J.-F.; San-Jose, P.; Prada, E.; Aguado, R.; Lee, E. J. H.; Gazibegovic, S.; Op het Veld, R. L. M.; Car, D.; Plissard, S. R.; Hocevar, M.; Pendharkar, M.; Lee, J. S.; Logan, J. A.; Palmstrøm, C. J.; Bakkers, E. P. A. M.; Frolov, S. M. Mirage Andreev Spectra Generated by Mesoscopic Leads in Nanowire Quantum Dots. *Phys. Rev. Lett.* **2018**, *121*, 127705.
(24) Estrada Saldaña, J. C.; Niquet, Y.-M.; Cleuziou, J.-P.; Lee, E. J. H.; Car, D.; Plissard, S. R.; Bakkers, E. P. A. M.; De Franceschi, S. Split-Channel Ballistic Transport in an InSb Nanowire. *Nano Lett.* **2018**, *18*, 2282−2287.
(25) Wang, Q.; Chen, Y.; Miao, L.; Jiang, G.; Chen, S.; Liu, J.; Fu, X.; Zhao, C.; Zhang, H. Wide Spectral and Wavelength-Tunable Dissipative Soliton Fiber Laser with Topological Insulator Nano-Sheets Self-Assembly Films Sandwiched by PMMA Polymer. *Opt. Express* **2015**, *23*, 7681−7693.
(26) Biegelsen, D. K.; Bringans, R. D.; Northrup, J. E.; Swartz, L.-E. Surface Reconstructions of GaAs(100) Observed by Scanning Tunneling Microscopy. *Phys. Rev. B* **1990**, *41*, 5701−5706.
(27) Arnoult, A.; Colin, J. Magnification Inferred Curvature for Real-Time Curvature Monitoring. *Sci. Rep.* **2021**, *11*, 9393.
(28) Dismukes, J. P.; Paff, R. J.; Smith, R. T.; Ulmer, R. Lattice Parameter and Density in Bismuth-Antimony Alloys. *J. Chem. Eng. Data* **1968**, *13*, 317−320.
(29) Cucka, P.; Barrett, C. S. The Crystal Structure of Bi and of Solid Solutions of Pb, Sn, Sb and Te in Bi. *Acta Crystallogr.* **1962**, *15*, 865−872.
(30) Xu, Y.; Miotkowski, I.; Liu, C.; Tian, J.; Nam, H.; Alidoust, N.; Hu, J.; Shih, C.-K.; Hasan, M. Z.; Chen, Y. P. Observation of Topological Surface State Quantum Hall Effect in an Intrinsic Three-Dimensional Topological Insulator. *Nat. Phys.* **2014**, *10*, 956−963.

https://doi.org/10.1021/acsami.1c08477
ACS Appl. Mater. Interfaces XXXX, XXX, XXX−XXX